Dalton Transactions

ROYAL SOCIETY OF CHEMISTRY

PAPER

View Article Online
View Journal | View Issue

Cite this: *Dalton Trans.*, 2023, **52**, 9622

Inherent area-selective atomic layer deposition of ZnS†

Chao Zhang, * Marko Vehkamäki, Markku Leskelä and Mikko Ritala

Atomic layer deposition processes with inherent substrate selectivity are more straightforward for area-selective atomic layer deposition (AS-ALD) than approaches using surface passivation or activation with self-assembled monolayers (SAMs), small molecule inhibitors (SMIs) or seed layers. Here, ALD of ZnS using elemental zinc and sulfur as precursors is reported to have excellent inherent selectivity. At 400–500 °C for 250 cycles, substantial ZnS growth was observed on Ti and TiO_2 surfaces while no growth was measured on native SiO_2 and Al_2O_3 surfaces. On TiO_2, the ZnS growth rate remains constant at 1.0 Å per cycle at temperatures of 400–500 °C. On Ti, in contrast, the initial growth rate increases significantly from 1.2 Å per cycle at 350 °C to 6.2 Å per cycle at 500 °C. The high growth rates on Ti are believed to be caused by CVD-like growth during the early ALD cycles, arising from the reservoir effect of the Ti layer for Zn atoms. After the first 100 cycles, the growth rate decreases from 3.5 to 1.0 Å per cycle, the same as the growth rate on TiO_2. Selective adsorption of sulfur on TiO_2 over Al_2O_3 and SiO_2 is assumed to be the selectivity mechanism on TiO_2. Self-aligned deposition of ZnS was successfully demonstrated on a micrometer-scale Ti/native SiO_2 pattern and on a nanometer-scale TiO_2/Al_2O_3 pattern at 450 °C for 250 cycles; ZnS films with a thickness of ~80 nm were selectively deposited on Ti over native SiO_2, and ZnS films with a thickness of ~23 nm were selectively deposited on TiO_2 over Al_2O_3.

Received 14th May 2023,
Accepted 15th June 2023

DOI: 10.1039/d3dt01435e

rsc.li/dalton

Introduction

With the continuation of device downsizing and the transition of device structures to more complex 3D architectures, such as FinFET and 3D NAND,[1] photolithography-based patterning has been facing unprecedented challenges. One of the critical challenges is to pattern state-of-the-art device features with accurate overlay control. Extreme ultraviolet (EUV) lithography and multiple patterning strategies are nowadays in use for high volume manufacturing (HVM) at the 5 nm technology node and beyond. In such advanced manufacturing processes involving very tight pitches, overlay misalignments of only a few nanometers lead to significant loss of device yield and thus become a major challenge for HVM.[2] Area-selective atomic layer deposition (AS-ALD) is considered a highly promising approach to mitigate this technical challenge.[3,4] Because of its capability to deposit a film only where needed in a self-aligned manner, AS-ALD provides a simple and cost-effective way for thin-film patterning without misalignment issues, even at the most critical feature sizes. Besides its great importance in semiconductor manufacturing, AS-ALD has also been studied for preparing high-performance catalysts with sophisticated nanostructures such as core–shell, non-continuous overcoating and embedded structures.[5]

To control film nucleation and growth so that the film materials are deposited only on the desired surface areas, the substrate surface can be modified before the ALD process. Surface modification is expected to either prevent the film growth by blocking reactive sites present on the substrate surface or to activate the film growth by creating reactive sites on the original nongrowth surface.[6] So far, most studies on AS-ALD have been conducted by using self-assembled monolayers (SAMs) with inert $-CH_3$ terminal groups as surface-passivation layers to prevent ALD growth.[7–9] As a result, film growth takes place only on the surface areas without SAMs while no growth occurs on the SAM-passivated areas. Although many successes have been achieved in AS-ALD by SAM-based surface passivation, the strict requirement for a densely packed SAM layer makes the SAM preparation time-consuming and defect-sensitive.[10,11] Also, the limited blocking ability of SAMs, along with their possible degradation at elevated temperatures, has limited their use in aggressive ALD processes.[12–14] SAM layers must also be removed after the deposition of the patterned layers. These limitations taken together have impeded the integration of SAM-based AS-ALD into industrial processes. Inert polymers have been studied as passivation layers for AS-ALD, although to a lesser extent compared to SAMs.[15–17] Recently,

Department of Chemistry, University of Helsinki, P.O. Box 55, 00014 Helsinki, Finland. E-mail: chao.zhang@helsinki.fi

† Electronic supplementary information (ESI) available. See DOI: https://doi.org/10.1039/d3dt01435e

AS-ALD using small molecular inhibitors (SMIs) has received increasing interest for self-aligned film patterning.[18–21] Because of their small sizes, SMIs are commonly more volatile than SAMs and can be easily vaporized and delivered under ALD conditions.

AS-ALD can also be realized by developing ALD processes that lead to immediate nucleation on certain substrate materials while a long nucleation delay is observed on others.[22] The nucleation differences result in selectivity during the initial ALD cycles. The so-called inherent substrate-dependent AS-ALD has received considerable research interest lately because it can potentially be used for fully self-aligned growth of thin-film patterns on semiconductor devices.[3] Generally speaking, three types of materials are used in semiconductor devices – conductors, semiconductors and dielectrics. Reactivities of these material surfaces towards ALD precursors can be different due to differences in surface terminations, catalytic activities or surface acidities. So far, only a few substrate-dependent AS-ALD processes have been reported due to the difficulty in designing or finding such ALD precursors with fine-tuned reactivity that would enable selective adsorption on target substrate materials while not on others. Catalytic materials enabling dissociative adsorption of O_2, such as Pt, Ir and RuO_x, have been used for AS-ALD of Ru, Pt, NiO and Fe_2O_3.[23–25] This selectivity is limited to those ALD processes that use O_2 as a co-reactant. Our work showed that CuO_x can be used as a catalytic seed layer for area-selective molecular layer deposition (AS-MLD) of polyimide at 200–210 °C.[26]

In addition to processes relying on the catalytic activities of substrate materials, different surface groups present on the substrate materials can be exploited to achieve AS-ALD. The most common case is selective deposition between hydrogen-terminated surfaces (such as Si:H, a-Si:H, a-SiN_x:H) and hydroxyl-terminated surfaces (SiO_2, metal oxides).[27–32] Hydroxyl groups are generally more reactive than hydrogen atoms towards ALD precursors. Thus, immediate nucleation usually occurs on oxide surfaces while there is a nucleation delay on H-terminated surfaces, which results in selective deposition on OH-terminated surfaces *versus* hydrogen-terminated surfaces during the initial ALD cycles. This selectivity typically lasts for only a few tens of ALD cycles, however, allowing selective deposition of a film with a thickness of only a few nanometers.

ZnS ALD from elemental zinc and sulfur has particular importance in the history of ALD since in 1974 Suntola *et al.* did their first ALD demonstrations using this process.[33] The original motivation to deposit ZnS by ALD was to develop a reliable production process for thin-film electroluminescent (TFEL) displays. Therefore, at that time, soda-lime glass was the major substrate material examined. The original process was soon replaced with the one using molecular precursors $ZnCl_2$ and H_2S because of their obvious advantages over the elemental precursors, such as much higher reactivity and volatility.[34] Subsequently, diethyl zinc was studied intensively for its higher volatility compared to $ZnCl_2$.[35] The high reactivity of precursors is important for most ALD applications where uniform films should be deposited at low temperatures, but on the other hand, it can be an obstacle for inherent AS-ALD. Therefore, ALD processes using less reactive elemental precursors, such as ZnS ALD from elemental zinc and sulfur, need to be investigated. Although not in use in current semiconductor devices, ZnS is important because it represents a group of interesting materials, metal chalcogenides, which have found a wide range of applications and attracted interest in optoelectronics, solar cells, fuel cells, sensors, memory devices, photodetectors and photocatalysis.[36] Also, ALD processes using elemental precursors enable deposition of film materials with high purity, which is especially important for semiconductors because impurities largely affect film properties, such as charge carrier mobility.

In this work, we have reinvestigated the ZnS ALD process using elemental zinc and sulfur as precursors. The growth behavior was studied on different substrate surfaces of evaporated Ti, ALD TiO_2, ALD Al_2O_3 and native SiO_2. Film properties including uniformity, stoichiometry and crystallinity were characterized by scanning electron microscopy (SEM), energy dispersive X-ray spectroscopy (EDX) and X-ray diffraction (XRD). Furthermore, ZnS deposition on the growth surfaces of Ti and TiO_2 and its nucleation on the nongrowth surfaces of native SiO_2 and Al_2O_3 were studied by SEM. Undesired nucleation on the nongrowth surfaces was decreased by optimizing the deposition temperature and precursor pulse time. Mechanistic understanding of the selectivity was also developed based on our experimental results and relevant information in the literature. In the end, self-aligned deposition of ZnS was demonstrated on a micrometer-scale Ti/native TiO_2 pattern and a nanometer-scale TiO_2/Al_2O_3 pattern.

Experimental section

Film deposition

ZnS thin films were grown in a hot-wall, cross-flow F120 ALD reactor (ASM Microchemistry). The reactor has an operating pressure of ~10 mbar with a continuous nitrogen flow through the reaction chamber. Nitrogen (N_2, AGA, 99.999%) was used as both the carrier and purge gas. Elemental zinc and sulfur, purchased from Sigma-Aldrich, were used as precursors to deposit ZnS films. Evaporation temperatures for Zn and S were 340 and 125 °C, respectively, and the precursor vapors were pulsed on the substrate with inert gas valving. ZnS films were deposited on four surfaces (Ti, TiO_2, native SiO_2 and Al_2O_3) at temperatures of 350–500 °C with different ALD cycle numbers. A Si wafer as such was used as the native SiO_2 surface. TiO_2 and Al_2O_3 surfaces were prepared by ALD. Anatase TiO_2 films with a thickness of 40 nm were deposited from $TiCl_4$ and water at 250 °C.[37] Amorphous Al_2O_3 with a thickness of ~80 nm was deposited from $AlCl_3$ and water at 300 °C.[38] A polycrystalline Ti surface was prepared by electron beam evaporation of 10 or 90 nm thick Ti layers on Si.

Preparation of Ti/native SiO_2 and TiO_2/Al_2O_3 patterns

Self-aligned ZnS deposition was tested on two patterned surfaces. A micrometer-scale Ti/native SiO_2 pattern, consisting of ~50 μm wide Ti lines and ~50 μm wide native SiO_2 spacers in between, was prepared by evaporating an ~10 nm thick Ti layer on a Si wafer through a shadow mask. A quartz crystal microbalance (QCM) was used to monitor the thickness of the deposited Ti layer. A nanometer-scale Al_2O_3/TiO_2 pattern was prepared from an Al_2O_3/TiO_2 laminate deposited by ALD on a Si wafer. The laminate cross-section, prepared by cleaving the sample carefully, was used as the patterned surface for the selectivity test. The widths of the TiO_2 and Al_2O_3 lines on the cross-sectioned surface correspond to the thicknesses of the TiO_2 (50 and 200 nm) and Al_2O_3 (200 and 350 nm) layers, respectively, in the laminate.

Film characterization

Thicknesses and stoichiometries of ZnS films were measured by energy-dispersive X-ray spectrometry (EDX) using a Hitachi S-4800 field emission scanning electron microscope (FESEM) equipped with an Oxford INCA 350 EDX spectrometer. The intensities of Kα X-ray lines from Zn and S, and ZnS bulk density of 4.090 g cm^{-3} were used for calculating film thicknesses by the GMRFILM program.[39] Film nucleation and growth were studied by SEM. The selective growth of ZnS was characterized by SEM and EDX mapping. Crystallinity was measured by using a Rigaku Smartlab X-ray diffractometer (XRD) utilizing Cu Kα-radiation with an incident angle of 1°.

Results and discussion

Selective deposition of ZnS on Ti and TiO_2 *versus* that on SiO_2 and Al_2O_3 surfaces

Substrate-dependent growth of ZnS was studied on Ti, TiO_2, native SiO_2 and Al_2O_3 surfaces at 350–500 °C for 250 ALD cycles. The observed growth rates were different on the studied surfaces, as shown in Fig. 1a. Over the examined temperature range, Ti is the surface with the highest growth rate, while TiO_2 comes second. The growth rates on native SiO_2 and Al_2O_3 are almost the same, although much lower than those on the other two surfaces. The growth rates on these surfaces are also temperature dependent. On 10 nm thick Ti, the growth rate increases from 1.2 to 6.2 Å per cycle as the deposition temperature increases from 350 to 500 °C. On TiO_2, the growth rate increases from 0.7 to 1.0 Å per cycle when the temperature is increased from 350 to 400 °C, and then remains at 1.0 Å per cycle up to 500 °C. In contrast, a decrease in the growth rate was measured on native SiO_2 and Al_2O_3. When the temperature increases to 400–500 °C, the growth rates decrease to zero on both surfaces. Therefore, selective deposition of ZnS on Ti and TiO_2 over native SiO_2 and Al_2O_3 becomes obvious at 400–500 °C.

Substrate-dependent selectivity in ALD processes arises from nucleation differences between the growth and non-growth surfaces, *i.e.*, long nucleation delays on the nongrowth surfaces and immediate nucleation with possible nucleation enhancement on the growth surfaces. Such nucleation differences can be identified by plotting film thicknesses as a function of the number of ALD cycles. Thicknesses of ZnS films deposited at 400 °C with 100, 250 and 500 ALD cycles were studied on 10 nm and 90 nm thick Ti, TiO_2, native SiO_2 and Al_2O_3. As shown in Fig. 1b, a long nucleation delay of at least 250 ALD cycles was measured on native SiO_2 and Al_2O_3. Linear growth with constant growth rate of 1 Å per cycle was measured on TiO_2, indicating immediate nucleation on TiO_2. Substrate-enhanced growth was observed on 10 nm and 90 nm thick Ti, as evidenced by the positive intercepts of the curves at the thickness axis (Fig. 1b). For the first 100 cycles, the growth rate is ~3.5 Å per cycle on 10 nm Ti and ~4.1 Å per cycle on 90 nm Ti. After that, the growth rates are ~1.0 Å per cycle, the same as that on TiO_2. The growth enhancement takes place only during the initial ALD cycles, and once the original Ti surfaces become fully covered with ZnS, further

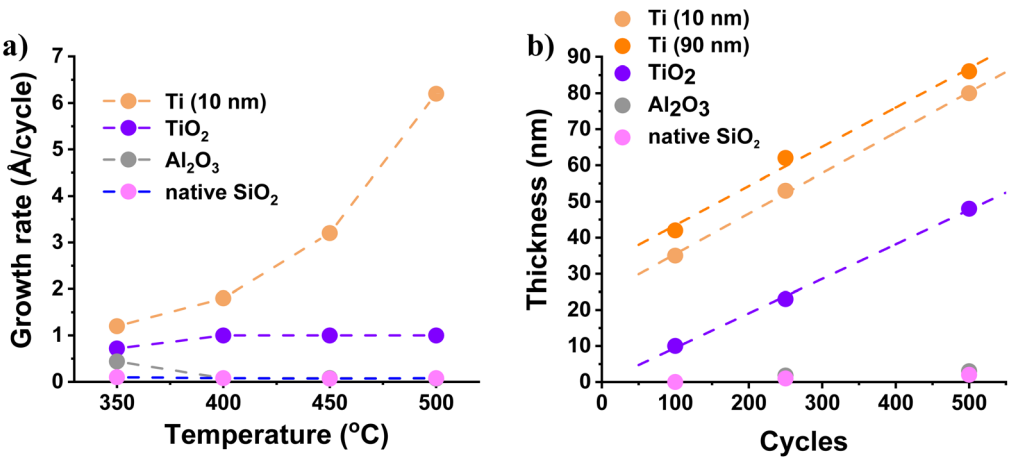

Fig. 1 (a) Growth rates *versus* deposition temperatures when the ALD cycle number was 250. (b) Film thicknesses *versus* cycle numbers when the depositions were conducted at 400 °C.

growth proceeds on deposited ZnS at a lower growth rate. The substrate-enhanced growth is assumed to be caused by the dissolution of Zn atoms into the Ti layers during the Zn pulses. Zn dissolution is a reversible process and after the Zn pulses the Ti layers function as Zn reservoirs, releasing Zn atoms and causing CVD-like growth during the S pulses. Larger growth rates are thus observed. Also, the initial growth rate on the 90 nm thick Ti (~4.1 Å per cycle) is larger than that on 10 nm Ti (~3.5 Å per cycle) because the thicker Ti layer allows more Zn dissolution. Similar CVD-like growth caused by Zn dissolution into growing Cu film was reported by Juppo *et al.*,[40] who studied Zn as a reducing agent for CuCl to deposit metallic copper by ALD. Zinc and titanium are known to form alloys with different compositions,[41,42] a process that supports the proposed dissolution mechanism.

Nucleation delays on Al_2O_3 and native SiO_2 and ZnS growth on Ti and TiO_2 were visualized from SEM images (Fig. 2). The ZnS ALD process was performed at 400 °C with 250, 500 and 1000 cycles on the nongrowth surfaces, and with 100, 250 and 500 cycles on the growth surfaces. No ZnS growth was observed on the Al_2O_3 surface for 250 ALD cycles while only minor nucleation was seen on native SiO_2. ZnS nucleation on Al_2O_3 and native SiO_2 is so slow that only isolated particles were observed even after 1000 ALD cycles. The estimated effective film thicknesses on Al_2O_3 and native SiO_2 were 3 and 5 nm, respectively, as measured by EDX. In contrast, already after 100 ALD cycles continuous ZnS films with thicknesses of 35 and 10 nm were deposited on Ti and TiO_2, respectively. Therefore, excellent selectivity of the ZnS ALD process at 400 °C was confirmed by SEM. As discussed above, on Ti the decrease of the ZnS growth rate with increasing ALD cycle numbers is ascribed to the covering of Ti surfaces by ZnS film. The SEM image in Fig. 2 confirms that the Ti surface was indeed fully covered already at 100 ALD cycles. Thereafter, the substrate-enhanced growth by Zn dissolution into the Ti layers was lost.

The substrate-enhanced growth of ZnS on Ti demonstrates a new way for AS-ALD. By utilizing the dissolution of ALD precursors into substrate materials, the film nucleation is signifi-

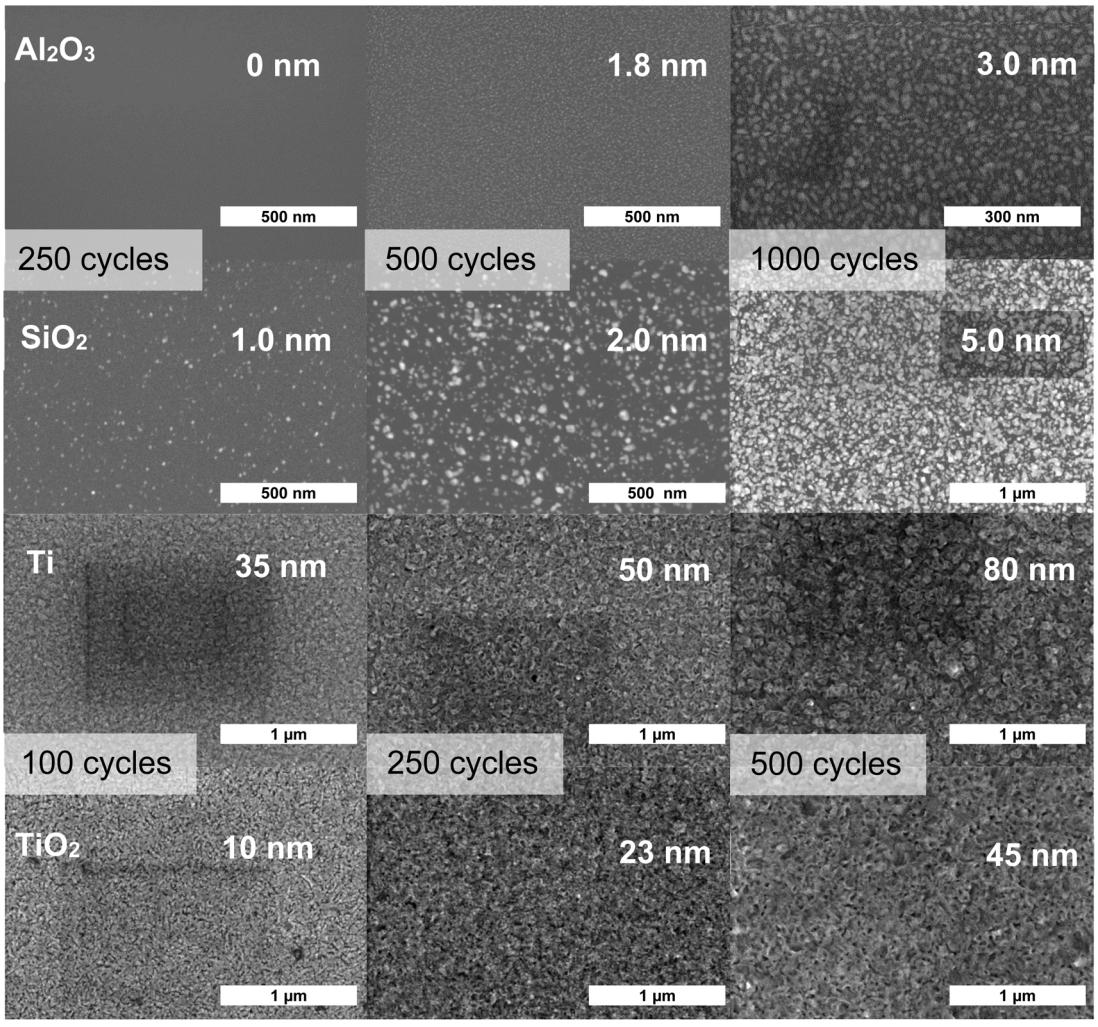

Fig. 2 SEM images of ZnS nucleation on Al_2O_3 and native SiO_2, and ZnS growth on Ti and TiO_2 at 400 °C. Insets: thicknesses of ZnS films. The darker contrast squares in some of the SEM images are surface contamination from focusing.

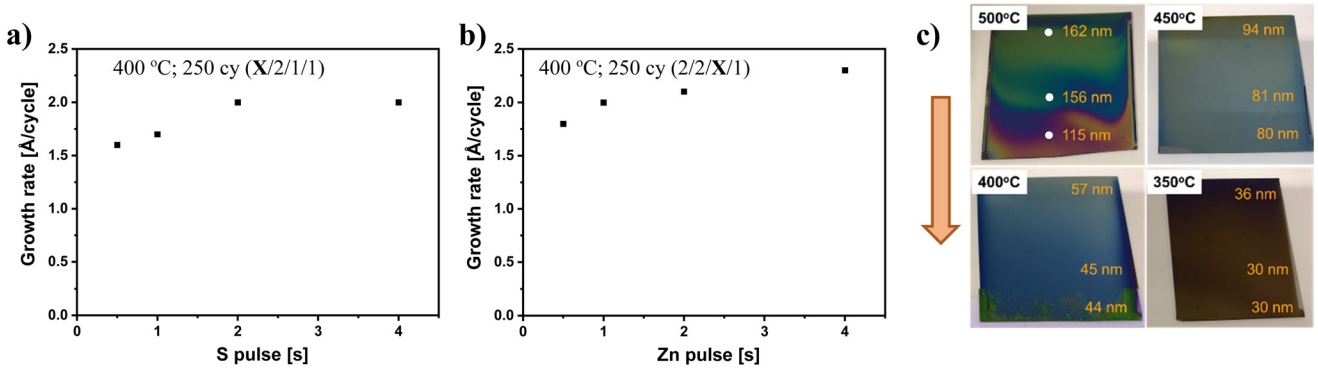

Fig. 3 Saturation curves of ZnS growth rates *versus* (a) S pulse times, and (b) Zn pulse times. (c) Photographs showing the uniformity of the ZnS thin films deposited on 10 nm Ti at various temperatures for 250 ALD cycles. The thicknesses were measured at the indicated point by EDX. The arrow indicates the direction of gas flow across the substrates.

cantly enhanced during the initial ALD cycles by a minor CVD-like growth. If at the same time the precursors desorb from other substrate materials, excellent selectivity can be achieved. The dissolution and CVD-like growth cannot be too extensive, however, as this would interfere with the ALD characteristics too much. In the studied case, ZnS growth was enhanced on Ti during the initial ALD cycles, while subsequent growth was able to continue in a typical ALD manner on the initially deposited ZnS. The merits of ALD were maintained at temperatures of 350–450 °C but were lost at the highest temperature of 500 °C (as seen below in Fig. 3c) due to too extensive Zn dissolution into the Ti layer. In contrast, no substantial ZnS growth was observed on Al_2O_3 and SiO_2 and the growth could not break through the nucleation stage even after 1000 cycles (Fig. 1b).

To explain the growth on TiO_2, another mechanism is needed. Long nucleation delay is commonly attributed to the inertness of substrate surfaces towards ALD precursors. Therefore, the precursors do not adsorb on the nongrowth surfaces. A previous study[43] showed that the adsorption of S_2 on Al_2O_3 is negligible at 27–427 °C, as measured by XPS. This was ascribed to an energy mismatch between the molecular orbitals of S_2 and the bands of Al_2O_3. The adsorption of sulfur on TiO_2 (110) was studied by Hebenstreit *et al.*[44] They observed that sulfur molecules adsorb easily on TiO_2 (110) at room temperature and at elevated temperatures. At room temperature, S_2 adsorbed dissociatively on the titanium rows of the surface, while at 300 °C the adsorption took place at the bridging oxygen rows through an S–O exchange. Therefore, selective adsorption of sulfur on TiO_2 over Al_2O_3 is proposed to be the mechanism for the selectivity between the TiO_2 and Al_2O_3 surfaces in the ZnS process. The same reasoning could be applied to explain the lack of growth on native SiO_2, *i.e.*, no adsorption of sulfur occurs on SiO_2.

Film quality of ZnS grown on Ti surface

As discussed above, the substrate-enhanced growth of ZnS on Ti is explained by the reversible dissolution of Zn atoms into the Ti layers and the consequent CVD-like growth during the initial ALD cycles, leading to an overall higher growth rate. This mechanism, however, did not affect the quality of the resulting films at deposition temperatures of 350–450 °C. Stoichiometric ZnS thin films with excellent uniformity were obtained on Ti-coated Si substrates with a size of 5 × 5 cm^2.

Although the ALD merit of self-limiting growth was most likely lost during the very first ALD cycles, it was restored once the Ti surface was fully covered with the deposited ZnS thin film, *i.e.*, the CVD-like growth caused by the out-diffused Zn from the Ti layer stopped as the ZnS growth proceeded. Indeed, reasonable saturation curves of ZnS growth rates *versus* S and Zn pulse times were achieved at 400 °C for 250 ALD cycles (Fig. 3). As seen in Fig. 3a, the growth rate was saturated at a 2 s sulfur pulse with a value of ~2.0 Å per cycle. Although the growth rate was not completely saturated with the Zn pulse time, only a slight increase was seen after 1 s Zn pulses; the measured growth rates were 2.0 Å per cycle at 1 s pulse, 2.2 Å per cycle at 2 s and 2.6 Å per cycle at 4 s (Fig. 3b). The self-limiting growth is therefore maintained at 400 °C for 250 cycles, as also supported by the excellent uniformity measured on the ZnS thin films deposited on the Ti layers at 350–450 °C (Fig. 3c). In contrast, a large thickness profile was observed on the film deposited at 500 °C (Fig. 3c). An obvious reason for the large thickness profile is that much more Zn dissolved into the Ti layer at 500 °C during the initial ALD cycles. During the S pulses, the S vapor was depleted at the leading edge of the substrate by reacting with out-diffusing Zn, leading to the growth of a film with a strong thickness profile. Also, a much higher growth rate of 6.5 Å per cycle was measured at 500 °C at the leading edge of the substrate, compared to 3.8 Å per cycle at 450 °C.

The stoichiometry and crystallinity of the ZnS films deposited on Ti at different temperatures were examined by EDX and XRD, respectively. The atomic ratios of Zn to S are consistent and within the accuracy of EDX, being close to 1 : 1 in the films deposited at all temperatures (Table 1), suggesting the growth of stoichiometric ZnS thin films. The corresponding EDX spectra are available in the ESI (Fig. S1†). The XRD patterns in Fig. 4 confirm that all the ZnS thin films deposited at

Table 1 Stoichiometry of the deposited ZnS films on Ti as measured with EDX

T_d (°C)	Zn, at%	S, at%
350	47	53
400	47	53
450	48	52
500	46	54

350–500 °C were polycrystalline. The wurtzite phase of ZnS was identified. The existence of the sphalerite phase cannot be ruled out, however, due to an overlap of the XRD patterns of the sphalerite and wurtzite phases. A weak diffraction peak at ~15° was detected from all the samples, possibly originating from crystalline TiS_2. The underlying Ti layers might be sulfurized by the S pulses during the initial ALD processes. We studied the change of the XRD patterns of the 10 nm Ti layer upon sulfur exposures at different temperatures. After 100 sulfur exposures, each consisting of a 2 s sulfur pulse and a 2 s N_2 purge, the diffraction peak at ~15° was detected at the examined temperatures and the peak intensity increased with increasing temperature. One could therefore argue that TiS_2 formation could explain film growth on Ti too, but because TiS_2 is a 2D material, its basal plane is inert and therefore a poor starting surface for film growth. Also, the substrate enhanced growth can only be explained by Zn dissolution into the Ti layer and therefore the latter is considered the dominant mechanism also for the selectivity.

Selectivity optimization

Insufficient selectivity is one of the main challenges in the development of AS-ALD processes. Limited selectivity arises from the undesired nucleation on the nongrowth surfaces, which becomes prominent during extended ALD cycles. In previous research, adsorption of precursors on the nongrowth surfaces has been suggested to be one reason for the loss of selectivity. Given that the precursor adsorption on the substrate surface is highly dependent on the deposition temperature and precursor pulse times, their effects on the ZnS nucleation on the nongrowth surface of native SiO_2 were studied to optimize the deposition conditions for the best selectivity. SEM was used to characterize the nucleation on native SiO_2 at various temperatures with different precursor pulse times.

ZnS nucleation on native SiO_2 at temperatures from 400 to 500 °C for 250 cycles is presented in the first row of SEM images in Fig. 5. Obviously, higher deposition temperatures result in fewer unwanted nuclei on SiO_2 due to the desorption of the precursors from the nongrowth surface. ZnS nucleation on SiO_2 with various Zn and S pulse times was studied at 400 °C for 250 cycles. As visualized in the second and third rows of SEM images in Fig. 5, longer precursor pulses generally lead to more ZnS nuclei on the nongrowth surface because more precursors can adsorb onto the surface compared to shorter precursor pulses. A long Zn pulse seems to cause more undesired ZnS nuclei, compared to long S pulses. To conclude, the selective deposition of ZnS was preferably conducted at high deposition temperatures with short precursor pulse times. Taking also film uniformity into account (Fig. 3c), the deposition temperature of 450 °C and 1 s precursor pulse times seem to be optimal for the AS-ALD of ZnS.

Selectivity demonstration on patterned samples

Self-aligned ALD of ZnS on Ti and TiO_2 over native SiO_2 and Al_2O_3 was successfully demonstrated on a micrometer-scale Ti/SiO_2 pattern and a nanometer-scale Al_2O_3/TiO_2 pattern. After 250 cycles at 450 °C, ~80 nm thick ZnS films were selectively deposited on the Ti regions while no detectable growth was measured on the SiO_2 regions, which is visualized from the SEM image, EDX map (Fig. 6a) and EDX spectra that were measured on the Ti and native SiO_2 regions, separately (Fig. S2†). On the nanometer-scale Al_2O_3/TiO_2 pattern, ~23 nm thick ZnS thin films were selectively deposited on the TiO_2 regions and no growth was observed on the Al_2O_3 regions, as characterized by SEM (Fig. 6b). Their selectivity is therefore excellent.

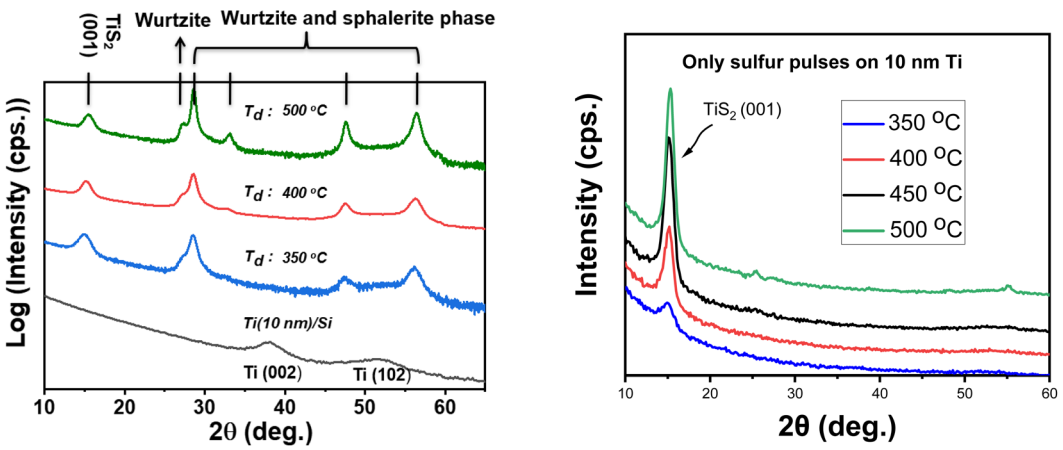

Fig. 4 XRD patterns of ZnS films deposited on 10 nm Ti at different temperatures (left). XRD patterns of the Ti layers after 100 pulses of sulfur with 2 s pulse and N_2 purge times (right).

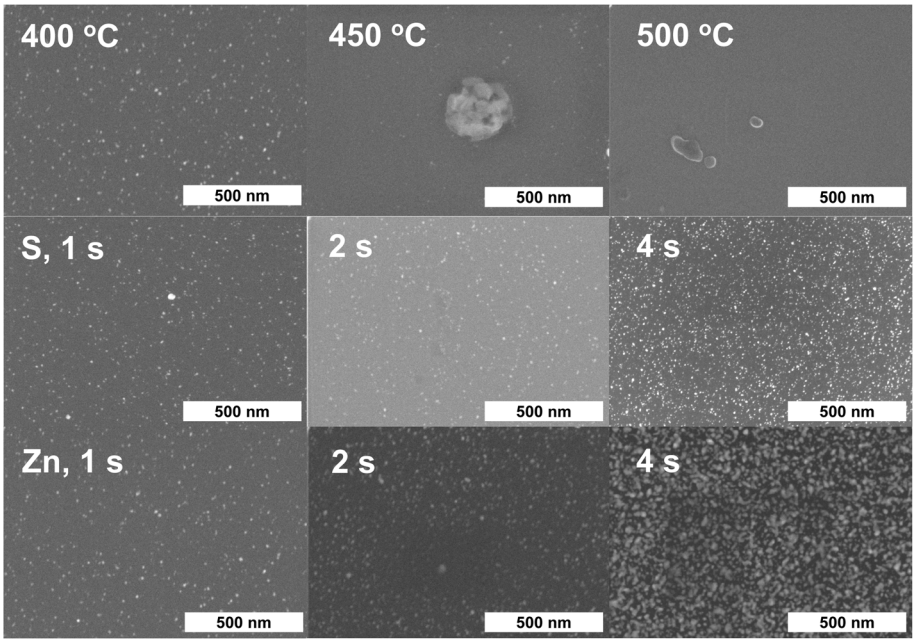

Fig. 5 SEM images demonstrating the effect of deposition temperatures and precursor pulse times on undesired film nucleation on the non-growth surface of native SiO_2.

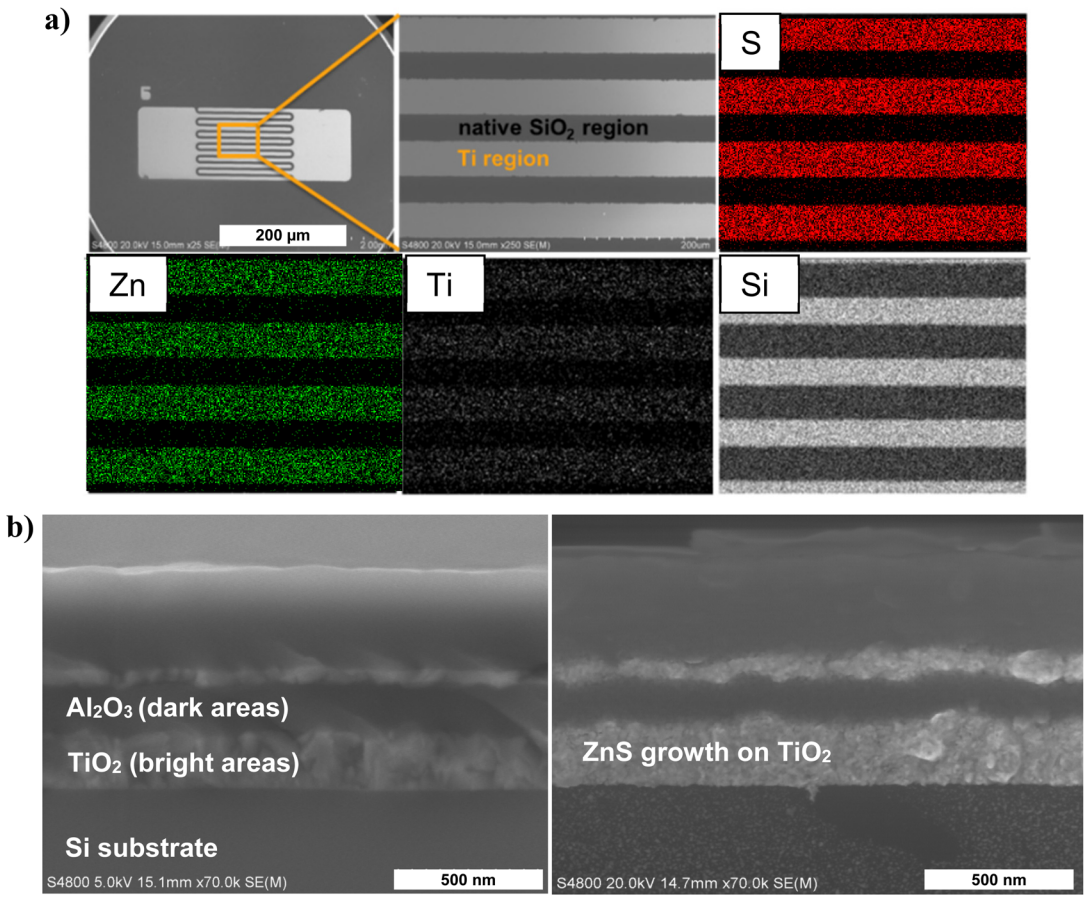

Fig. 6 Selectivity demonstrations on (a) the micrometer-scale Ti/native SiO_2 patterns and (b) the nanometer-scale TiO_2/Al_2O_3 patterns.

Conclusion

In the present work, we investigated the ZnS ALD process using elemental Zn and S as precursors for AS-ALD. Our study showed that excellent selective growth of ZnS on Ti and TiO_2 surfaces with respect to native SiO_2 and Al_2O_3 surfaces can be achieved at deposition temperatures of 400–450 °C. Substrate-enhanced growth was observed on Ti, which is ascribed to the reservoir effect of the Ti layer for Zn atoms during the first ALD cycles. Slight CVD-like growth is expected to occur due to reactions between out-diffusing Zn and sulfur during the sulfur pulses. The ALD merit was maintained at temperatures of 350–450 °C with very uniform films grown on 10 nm Ti films but was lost at the highest temperature of 500 °C with a large thickness profile in the resulting films, which is likely due to too extensive Zn dissolution into the Ti layers. At 400 °C, the ZnS growth was enhanced during the first 100 ALD cycles with an average growth rate of 3.5 Å per cycle, while the subsequent growth continued in a typical ALD manner on deposited ZnS with a growth rate of 1.0 Å per cycle. Linear growth with a growth rate of 1.0 Å per cycle was measured on TiO_2 while no ZnS growth was detected on Al_2O_3 and native SiO_2 and the growth could not break through the nucleation stage even after 1000 cycles. Based on our results and literature knowledge, selective adsorption of sulfur on TiO_2 over Al_2O_3 and SiO_2 is proposed to be the selectivity mechanism on the oxide surfaces. In the end, self-aligned deposition of ZnS was successfully demonstrated on a micrometer-scale Ti/native SiO_2 pattern and a nanometer-scale TiO_2/Al_2O_3 pattern at 450 °C for 250 cycles; ZnS films with a thickness of ~80 nm were selectively deposited on Ti over native SiO_2, and ZnS films with a thickness ~23 nm were selectively deposited on TiO_2 over Al_2O_3.

Author contributions

Conceptualization: C. Z., M. V. and M. R. Data curation: C. Z. Formal analysis: C. Z. Funding acquisition: M. R. and C. Z. Investigation: C. Z. Methodology: C. Z. Project administration: C. Z. Resources: C. Z., M. L. and M. R. Software: C. Z. Supervision: M. R. and M. L. Validation: C. Z. Visualization: C. Z. Writing – original draft preparation: C. Z. Writing – review and editing: C. Z., M. V., M. L. and M. R.

Conflicts of interest

There are no conflicts to declare.

Acknowledgements

Financial support from the Academy of Finland (decision number 338707) and the China Scholarship Council (file no. 201507040043) is gratefully acknowledged. The authors thank Marianna Kemell for the discussion on SEM measurements and Mikko Heikkila for the discussion on XRD measurements. This work was done at the ALD Centre Finland research infrastructure.

References

1 International Roadmap for Devices and Systems (IRDS) 2022 Edition White Papers, https://irds.ieee.org/editions/2022, (accessed 2023-01-06).
2 N. Mohanty, J. T. Smith, L. Huli, C. Pereira, A. Raley, S. Kal, C. Fonseca, X. Sun, R. L. Burns and R. A. Farrell, 2017. SPIE Advanced Lithography 2017, **10147**, 1014704.
3 R. Clark, K. Tapily, K. H. Yu, T. Hakamata, S. Consiglio, D. O'Meara, C. Wajda, J. Smith and G. Leusink, *APL Mater.*, 2018, **6**, 058203.
4 G. N. Parsons and R. D. Clark, *Chem. Mater.*, 2020, **32**, 4920–4953.
5 K. Cao, J. M. Cai and R. Chen, *Chem. Mater.*, 2020, **32**, 2195–2207.
6 A. J. M. Mackus, A. A. Bol and W. M. M. Kessels, *Nanoscale*, 2014, **6**, 10941–10960.
7 E. Farm, M. Kemell, M. Ritala and M. Leskela, *Thin Solid Films*, 2008, **517**, 972–975.
8 R. Chen and S. F. Bent, *Adv. Mater.*, 2006, **18**, 1086–1090.
9 T. L. Liu and S. F. Bent, *Chem. Mater.*, 2021, **33**, 513–523.
10 R. Chen, H. Kim, P. C. McIntyre and S. F. Bent, *Chem. Mater.*, 2005, **17**, 536–544.
11 R. Chen, H. Kim, P. C. McIntyre and S. F. Bent, *Appl. Phys. Lett.*, 2004, **84**, 4017–4019.
12 M. Pasquali, P. Carolan, S. Sergeant, J. Meersschaut, V. Spampinato, T. Conard, A. Viva, S. De Gendt and S. Armini, *ACS Appl. Electron. Mater.*, 2022, **4**, 1703–1714.
13 A. Brady-Boyd, R. O'Connor, S. Armini, V. Selvaraju, M. Pasquali, G. Hughes and J. Bogan, *Appl. Surf. Sci.*, 2022, **586**, 152679.
14 H. B. R. Lee, J. Kim, H. Kim, W. H. Kim, J. W. Lee and I. Hwang, *J. Korean Phys. Soc.*, 2010, **56**, 104–107.
15 E. Farm, M. Kemell, M. Ritala and M. Leskela, *J. Phys. Chem. C*, 2008, **112**, 15791–15795.
16 E. Farm, M. Kemell, E. Santala, M. Ritala and M. Leskela, *J. Electrochem. Soc.*, 2010, **157**, K10–K14.
17 A. Sinha, D. W. Hess and C. L. Henderson, *J. Electrochem. Soc.*, 2006, **153**, G465–G469.
18 J. Yarbrough, A. B. Shearer and S. F. Bent, *J. Vac. Sci. Technol., A*, 2021, **39**, 021002.
19 M. J. M. Merkx, S. Vlaanderen, T. Faraz, M. A. Verheijen, W. M. M. Kessels and A. J. M. Mackus, *Chem. Mater.*, 2020, **32**, 7788–7795.
20 H. G. Kim, M. Kim, B. Gu, M. R. Khan, B. G. Ko, S. Yasmeen, C. S. Kim, S. H. Kwon, J. Kim, J. Kwon, K. Jin, B. Cho, J. S. Chun, B. Shong and H. B. R. Lee, *Chem. Mater.*, 2020, **32**, 8921–8929.
21 A. Mameli, M. J. M. Merkx, B. Karasulu, F. Roozeboom, W. M. M. Kessels and A. J. M. Mackus, *ACS Nano*, 2017, **11**, 9303–9311.

22 A. J. M. Mackus, M. J. M. Merkx and W. M. M. Kessels, *Chem. Mater.*, 2019, **31**, 2–12.
23 J. A. Singh, N. F. W. Thissen, W. H. Kim, H. Johnson, W. M. M. Kessels, A. A. Bol, S. F. Bent and A. J. M. Mackus, *Chem. Mater.*, 2018, **30**, 663–670.
24 A. J. M. Mackus, N. F. W. Thissen, J. J. L. Mulders, P. H. F. Trompenaars, M. A. Verheijen, A. A. Bol and W. M. M. Kessels, *J. Phys. Chem. C*, 2013, **117**, 10788–10798.
25 E. Färm, S. Lindroos, M. Ritala and M. Leskelä, *Chem. Mater.*, 2012, **24**, 275–278.
26 C. Zhang, M. Vehkamaki, M. Pietikainen, M. Leskela and M. Ritala, *Chem. Mater.*, 2020, **32**, 5073–5083.
27 M. M. Minjauw, H. Rijckaert, I. Van Driessche, C. Detavemier and J. Dendooven, *Chem. Mater.*, 2019, **31**, 1491–1499.
28 J. S. Kim and G. N. Parsons, *Chem. Mater.*, 2021, **33**, 9221–9230.
29 P. C. Lemaire, M. King and G. N. Parsons, *J. Chem. Phys.*, 2017, **146**, 052811.
30 S. E. Atanasov, B. Kalanyan and G. N. Parsons, *J. Vac. Sci. Technol., A*, 2016, **34**, 01A148.
31 B. Kalanyan, P. C. Lemaire, S. E. Atanasov, M. J. Ritz and G. N. Parsons, *Chem. Mater.*, 2015, **28**, 117–126.
32 H. M. Kim, J. H. Lee, S. H. Lee, R. Harada, T. Shigetomi, S. Lee, T. Tsugawa, B. Shong and J. S. Park, *Chem. Mater.*, 2021, **33**, 4353–4361.
33 T. Suntola and J. Antson, *U.S. Patent*, 4058430, 1977.
34 M. Pessa, R. Makela and T. Suntola, *Appl. Phys. Lett.*, 1981, **38**, 131–132.
35 E. B. Yousfi, T. Asikainen, V. Pietu, P. Cowache, M. Powalla and D. Lincot, *Thin Solid Films*, 2000, **361**, 183–186.
36 X. S. Fang, T. Y. Zhai, U. K. Gautam, L. Li, L. M. Wu, B. Yoshio and D. Golberg, *Prog. Mater. Sci.*, 2011, **56**, 175–287.
37 M. Ritala, M. Leskela, E. Nykanen, P. Soininen and L. Niinisto, *Thin Solid Films*, 1993, **225**, 288–295.
38 L. Hiltunen, H. Kattelus, M. Leskelä, M. Mäkelä, L. Niinistö, E. Nykänen, P. Soininen and M. Tiittad, *Mater. Chem. Phys.*, 1991, **28**, 379–388.
39 R. Waldo, *Microbeam Anal.*, 1988, 310–314.
40 M. Juppo, M. Ritala and M. Leskela, *J. Vac. Sci. Technol., A*, 1997, **15**, 2330–2333.
41 J. L. Murray, *Bull. Alloy Phase Diagrams*, 1984, **5**, 52–56.
42 G. P. Vassilev, X. J. Liu and K. Ishida, *J. Alloys Compd.*, 2004, **375**, 162–170.
43 J. A. Rodriguez and M. Kuhn, *J. Phys. Chem. B*, 1997, **101**, 3187–3195.
44 E. L. D. Hebenstreit, W. Hebenstreit and U. Diebold, *Surf. Sci.*, 2000, **461**, 87–97.